Anisotropic superexchange and spin-resonance linewidth in diluted magnetic semiconductors

B. E. Larson
Department of Physics, Boston University, Boston, Massachusetts 02215

H. Ehrenreich
Division of Applied Sciences and Department of Physics, Harvard University, Cambridge, Massachusetts 02138

(Received 8 June 1988)

The Dzyaloshinski-Moriya (DM) anisotropic superexchange constant and the resulting electron-paramagnetic-resonance (EPR) linewidth in Mn-based II-VI-compound diluted magnetic semiconductors (DMS) such as $Cd_{1-x}Mn_xTe$ are calculated quantitatively. An Anderson Hamiltonian, developed in a previous study of isotropic superexchange, describing correlated Mn $3d$ states hybridized with semiconducting s- and p-derived levels, is generalized to include the *anion* spin-orbit coupling responsible for anisotropic superexchange. DM exchange is shown to be the dominant anisotropic interaction, with magnitude $\sim 5\%$ of isotropic superexchange. The EPR line shape is calculated with use of a moment expansion of the magnetic response function to first order in inverse temperature together with a maximum-entropy ansatz. The calculated infinite-temperature linewidths are in good agreement with extrapolated experimental values. A novel fit of the theoretical temperature dependence to existing experimental linewidth data provides the first empirical value for the anisotropic exchange constant, in excellent agreement with the theoretical value. Calculated chemical trends for the exchange constants yield the experimentally expected linewidth trends.

I. INTRODUCTION

We establish by quantitative calculation the existence of significant anisotropic superexchange having the Dzyaloshinski-Moriya (DM) form in Mn-based II-VI-compound diluted magnetic semiconductors (DMS) such as $Cd_{1-x}Mn_xTe$. The high-temperature electron-paramagnetic-resonance (EPR) linewidth[1] is calculated quantitatively. Anisotropic superexchange is shown to be predominantly responsible for the linewidth. The analytic form of the expression for the temperature-dependent linewidth yields the first empirical value for the anisotropic coupling constant through a novel fit to existing experimental linewidth data.[2]

The Mn-Mn exchange is described by the effective spin Hamiltonian

$$H_{\rm spin}=-\sum_{i\neq j}{}'\sum_{\alpha,\beta} S_{i\alpha}\mathcal{J}_{\alpha\beta}(\mathbf{R}_{ij})S_{j\beta}=H_H+H_{\rm DM}\ . \tag{1.1}$$

Here $S_{i\alpha}$ is the αth component ($\alpha=x,y,z$) of the Mn spin ($S=\frac{5}{2}$) at site $\mathbf{R}_i$, and $\mathbf{R}_{ij}=\mathbf{R}_j-\mathbf{R}_i$. The prime indicates that only Mn-occupied sites are to be included. [With our convention the total interaction between two spins is $-2\sum_{\alpha,\beta}\mathcal{J}_{\alpha\beta}(\mathbf{R}_{12})S_{1\alpha}S_{2\beta}$.] The dominant interactions[3,4] contained in the *exchange tensor* $\mathcal{J}_{\alpha\beta}(\mathbf{R}_{ij})$ are isotropic exchange $J(\mathbf{R}_{ij})$ described by the Heisenberg Hamiltonian H_H,

$$H_H=-\sum_{i\neq j}{}' J(\mathbf{R}_{ij})\mathbf{S}_i\cdot\mathbf{S}_j,\quad J(\mathbf{R}_{ij})\equiv\tfrac{1}{3}\sum_{\alpha}\mathcal{J}_{\alpha\alpha}(\mathbf{R}_{ij})\ , \tag{1.2}$$

and when significant spin-orbit interactions are present, the Dzyaloshinsky-Moriya anisotropic exchange,[4-7]

$$H_{\rm DM}=-\sum_{i\neq j}{}'\mathbf{D}(\mathbf{R}_{ij})\cdot\mathbf{S}_i\times\mathbf{S}_j,\quad D_\alpha\equiv\tfrac{1}{2}\sum_{\beta\gamma}\varepsilon_{\alpha\beta\gamma}\mathcal{J}_{\beta\gamma}(\mathbf{R}_{ij})\ . \tag{1.3}$$

Here $\varepsilon_{\alpha\beta\gamma}$ is the completely antisymmetric third-rank Levi-Cività tensor. The rapid decay with distance of the exchange constants[8] permits restricting the sum to nearest neighbors (NN) only. The isotropic exchange constant for nearest neighbors, J_1, is ~ -10 K in DMS,[9,10] and arises almost entirely from superexchange. Anisotropic superexchange in DMS has not been calculated or measured previously. Significant anisotropic Mn-Mn exchange is expected to be of importance for understanding the properties of the presumed DMS spin-glass phase,[11-13] and may give insight into switching times of DMS-based magneto-optical devices.[14]

The calculation of D_1 (Sec. II), follows closely the formalism described in a preceding paper[8] for isotropic superexchange.[15] The starting point is a microscopic Anderson Hamiltonian, parametrized from experiment, describing correlated Mn $3d$ states hybridized with semiconducting s and p-derived levels. The sp bands are modeled using a semiempirical tight-binding formalism.[16] A single new tight-binding parameter characterizes the anion spin-orbit coupling. The novel effect of the *anion* spin-orbit coupling in causing NN anisotropic interactions in a nonmetal is similar to the mechanism generating long-ranged DM interactions in metals.[17] Well-studied magnetic nonmetals like MnO and $KMnF_3$ involve anions with atomic numbers Z and associated spin-orbit couplings $\sim Z^2$ which are smaller than those of the first transition series,[18] or possess crystalline phases with sufficiently high symmetry to exclude DM interac-

tions. The only previous realistic calculations of DM exchange for a nonmetal were those of Pearson for β-MnS.[19] The inclusion there of Mn spin-orbit interactions led to complexities preventing the results from having more than order-of-magnitude accuracy. By contrast, our D_1 calculations benefit from the simplifying neglect of Mn spin-orbit interactions relative to those of the anion.

We calculate J_1 and D_1 microscopically by exploiting the equivalence for the ground-state manifold between the Anderson Hamiltonian and $H_{\rm spin}$ [Eq. (1.1)]. Brillouin zone sums are evaluated using the special k-points method,[20,21] avoiding the spherical approximations made in Ref. 8. The calculated $J_1=-5.6$ K for $Cd_{1-x}Mn_xTe$ is in excellent agreement with experiment. We find $D_1=0.3$ K for $Cd_{1-x}Mn_xTe$, and calculate chemical trends in J_1 and D_1 for other DMS, using parameters determined for a three-level model developed in Ref. 8, with anion spin-orbit parameters obtained from published tight-binding parametrizations for CdTe, CdSe, and CdS.[22] Comparison with other anisotropic interactions establishes DM exchange to be the dominant microscopic anisotropy. This fact has direct implications for EPR linewidths.

The high-temperature EPR line is exchange narrowed,[23–25] due to the large size of J_1 relative to anisotropic interactions. Experiments show that the linewidth decreases by almost an order of magnitude through the anion series: Te,Se,S.[26,27] Samarth and Furdyna[27] showed that the magnetic dipole-dipole interaction could not explain the magnitude or trend of the linewidth, and suggested DM exchange might be responsible. We develop a quantitative theory of linewidths and linewidth trends.

Our EPR calculation (Sec. III) makes use of a number of previously developed techniques. We compute the first two nonvanishing frequency moments[25,28,29] of the microscopic magnetic response and memory functions and their first-order inverse temperature corrections using the calculated exchange and NN dipole-dipole interactions. The line shape is obtained from the moments using the maximum-entropy method.[30–33] A detailed account of these calculations is given in Ref. 2.

We find the temperature-dependent linewidth $\Delta H(T)$ is given by

$$\Delta H(T)=\Delta H_\infty\left[1+\frac{\Theta_d+\Theta_p}{T}\right]. \tag{1.4}$$

Here ΔH_∞ is the infinite temperature linewidth, Θ_p is the experimental paramagnetic Curie temperature, and Θ_d is a spin temperature to be discussed below. We calculate ΔH_∞ for $Cd_{1-x}Mn_xB^{\rm VI}$ ($B^{\rm VI}$=Te,Se,S). The results confirm the experimental anion trend and yield $\sim 30\%$ agreement with the extrapolated experimental ΔH_∞ values. Equation (1.4) is also used in a novel reanalysis of the experimental linewidth data which regards the theoretical quantities $(\Delta H_\infty,\Theta_d)$ as parameters to be fit by experiment.[34] Values of ΔH_∞ from 12 $Cd_{1-x}Mn_xTe$ samples[27,35,36] ranging from $x=0.12$ to $x=0.53$ yield the first empirical value of the DM coupling constant $D_1=0.28\pm0.03$ K in excellent agreement with the (independent) theoretical value. The good agreement validates the theoretical framework developed previously[2,8] which is extended here.

II. ANISOTROPIC SUPEREXCHANGE

A. Model Hamiltonian and calculation

The calculation of DM exchange for $Cd_{1-x}Mn_xTe$ starts from a consideration of the necessary relativistic modifications to the electronic structure. As in Ref. 8 the important features of the electronic structure are subsumed by a model Hamiltonian for calculating magnetic properties. The electronic structure is based on relativistic empirical-tight-binding–coherent-potential-approximation (ETB-CPA) calculations. For $Hg_{1-x}Cd_xTe$ (Ref. 16) and $Hg_{1-x}Mn_xTe$ (Ref. 37) these calculations achieved good agreement with experimental values of the valence-band Γ_8-Γ_7 splitting, which depends crucially on spin-orbit interactions. More recent ETB-CPA calculations for $Cd_{1-x}(Mn\uparrow)_{x/2}(Mn\downarrow)_{x/2}Te$ show that the location and hybridization of spin-split Mn $3d$ states is largely unaffected by spin-orbit effects.[38–40] Mn is relatively light ($Z=25$), so relativistic effects are small. The main relativistic effects associated with the sp valence-band states are (1) a uniform shift to lower energy due to the mass-velocity term (estimated to be ~ 0.4 eV)[8] and (2) a spin-orbit splitting of the sixfold-degenerate Γ_{15} into a higher-energy quartet Γ_8 and lower doublet Γ_7. The ETB-CPA results indicate that the important features of the alloy electronic structure are well represented by the virtual-crystal approximation (VCA). This follows from the local character of the exchange constants, their predominant dependence on anion-derived intermediate states, and the lack of disorder on the anion sublattice. In position space, a nearest-neighbor (NN) exchange process between two Mn atoms involves principally the single intervening (Te) anion. The disordered occupation of other cation sites is therefore of little consequence.

A model Hamiltonian suitable for calculating anisotropic exchange is

$$H=H_0+H_d+H_{pd}\ , \tag{2.1}$$

where

$$H_0=\sum_{\mu,\mathbf{k}}\varepsilon_\mu(\mathbf{k})a^\dagger_{\mu\mathbf{k}}a_{\mu\mathbf{k}} \tag{2.2}$$

describes the sp electronic structure. Here $a^\dagger_{\mu\mathbf{k}}$ creates an electron in band μ with wave vector $\mathbf{k}$ in Bloch state $|\mu\mathbf{k}\rangle$. Since the spin-orbit potential mixes spins, the state $|\mu\mathbf{k}\rangle$ is a linear combination of spin-up and spin-down components. As before, the $\varepsilon_\mu(\mathbf{k})$ are calculated using the ETB-VCA with a basis of one cation (Mn or Cd) s orbital and three anion (Te) p orbitals.[8] Except for the introduction of the spin-orbit interaction $\lambda_a=\langle p_x|(\hbar/4m^2c^2r)(\partial V/\partial r)|p_x\rangle$, and a compensating $\sim 10\%$ x-independent shift of the cation on-site energy, the electronic parameters have the same values as those used for the ETB-VCA bands in Ref. 8. $V(\mathbf{r})$ in λ_a is some op-

timal one-electron crystal potential in anion-centered coordinates, which is spherically symmetric sufficiently near the anion nucleus $\mathbf{r}=\mathbf{0}$. $|p_x\rangle$ is the p_x-symmetry basis function on the anion.

$$H_d=\sum_i{}' \sum_{m,\sigma} (\varepsilon_d+U_{\rm eff}\langle n_{im-\sigma}\rangle)n_{im\sigma} \tag{2.3}$$

describes five Mn d electrons per site with site-localized linearized correlations. Here $n_{im\sigma}=d^\dagger_{im\sigma}d_{im\sigma}$ and $d^\dagger_{im\sigma}$ creates a d electron of spin σ at Mn site i in state $|im\sigma\rangle$ having e_g or t_{2g} symmetry within the zinc-blende point group. We use the primed sum to indicate that only Mn-occupied sites are included. Mn spin-orbit interactions are neglected. The Hamiltonian of Eq. (2.3) is assumed to act on a subspace of d^4, d^5, or d^6 configurations (per site).[41] The parameters ε_d and $U_{\rm eff}$ can be regarded to be m independent, and take the values -3.4 eV (relative to the valence-band-edge energy zero at E_V), and 7.0 eV, respectively. However, in computing the vector quantity $\mathbf{D}(\mathbf{R}_{ij})$, accurate account must be taken of the point symmetry of different d orbitals. Thus the form of H_d differs from that used in Ref. 8 in that the full symmetry of the d functions is taken into account. As before we assume $\langle n_{im\sigma}\rangle=0,1$, in accord with Hund's rule and with the experimental moment of $5\mu_B$.[42]

$$H_{pd}=\sum_i{}' \sum_{m,\sigma} \sum_{\mu,\mathbf{k}} [\tilde V_{pd}(\mu,\mathbf{k};m,\sigma)e^{i\mathbf{k}\cdot\mathbf{R}_i}d^\dagger_{im\sigma}a_{\mu\mathbf{k}}+\text{H.c.}] \tag{2.4}$$

describes hybridization of Mn d with sp band states. The k-dependent hybridization functions $\tilde V_{pd}(\mu,\mathbf{k};m,\sigma)\equiv\langle m\sigma|H|\mu\mathbf{k}\rangle$ are given within the ETB-VCA model described above by

$$\begin{aligned}\tilde V_{pd}(\mu,\mathbf{k};m,\sigma)&=N^{-1/2}\sum_{\alpha=p_x,p_y,p_z}\langle\alpha\mathbf{k}\sigma|\mu\mathbf{k}\rangle[(pd\sigma)A^\alpha_m(\mathbf{k})\\&\quad+(pd\pi)B^\alpha_m(\mathbf{k})]\ .\end{aligned} \tag{2.5}$$

Here $|\alpha\mathbf{k}\sigma\rangle$ is the ket corresponding to a spin-σ Bloch sum of orbital α on the Te anions. The functions $A^\alpha_m(\mathbf{k})$ and $B^\alpha_m(\mathbf{k})$ have the $\mathbf{k}$ dependence familiar from tight-binding theory.[2] These functions are independent of the hopping parameters and have the same form for any zinc-blende crystal. The *spin-parallel* position-space Slater-Koster hopping parameters are $(pd\sigma)$ and $(pd\pi)$ in the two-center approximation.[43] The ratio $(pd\sigma)/(pd\pi)$ is assumed to have the constant value -2.18 (with $(pd\sigma)<0$) in agreement with Harrison's scaling rule according to which both $(pd\sigma)$ and $(pd\pi)$ vary as $d^{-7/2}$ with distance d.[44] The values $(pd\sigma)$ and $(pd\pi)$ are then determined by noting that the experimentally measured valence-band-edge sp-d exchange constants $N\beta$ ($=-0.88$ eV) (Ref. 45) provide the linear combination[8]

$$N\beta=-\tfrac{32}{5}[\tfrac{1}{3}(pd\sigma)-\tfrac{2}{3}(pd\pi)]^2\times[(E_V-\varepsilon_d)^{-1}+(U_{\rm eff}+\varepsilon_d-E_V)^{-1}]\ . \tag{2.6}$$

The ground state of the Hamiltonian H_0+H_d has a degeneracy of $2S+1$ per site corresponding to different orientations of the Mn spin-$\frac{5}{2}$ moments. This degeneracy is partially lifted by the perturbation H_{pd}. The resulting spectrum of weakly excited states is described by the effective spin Hamiltonian $H_{\rm spin}$ [Eq. (1.1)]. $H_{\rm spin}$ is equivalent to H [Eq. (2.1)] in all respects within the ground-state manifold. Following Anderson and Moriya, we assume that the most important terms in $H_{\rm spin}$ are H_H [Eq. (1.2)] and $H_{\rm DM}$ [Eq. (1.3)].

The exchange constants are calculated by a generalization of the method used in Ref. 8. First, the Hamiltonian [Eq. (1.1)] is expressed in a more convenient form using the operators $S_{i\pm}\equiv S_{ix}\pm iS_{iy}$,

$$\begin{aligned}H_{\rm spin}=-\sum_{i\neq j}{}'\Big\{&J(\mathbf{R}_{ij})[S_{iz}S_{jz}+\tfrac{1}{2}(S_{i+}S_{j-}+S_{i-}S_{j+})]\\&-\frac{i}{2}D_z(\mathbf{R}_{ij})(S_{i-}S_{j+}-S_{i+}S_{j-})\\&+\frac{i}{2}D_-(\mathbf{R}_{ij})(S_{iz}S_{j+}-S_{i+}S_{jz})\\&-\frac{i}{2}D_+(\mathbf{R}_{ij})(S_{iz}S_{j-}-S_{i-}S_{jz})\Big\}\ .\end{aligned} \tag{2.7}$$

The exchange constants appearing in the spin Hamiltonian (2.7) are given by

$$J(\mathbf{R}_{ij})=-(4S)^{-1}(\langle S-1,S|H_{\rm spin}|S,S-1\rangle+\langle S,S-1|H_{\rm spin}|S-1,S\rangle)\ , \tag{2.8}$$

$$\begin{aligned}D_z(\mathbf{R}_{ij})&=(4iS)^{-1}(\langle S-1,S|H_{\rm spin}|S,S-1\rangle-\langle S,S-1|H_{\rm spin}|S-1,S\rangle)\ ,\\D_-(\mathbf{R}_{ij})&=i(S\sqrt{2S})^{-1}\langle S,S|H_{\rm spin}|S,S-1\rangle\ ,\end{aligned} \tag{2.9}$$

and

$$D_+(\mathbf{R}_{ij})=i(S\sqrt{2S})^{-1}\langle S-1,S|H_{\rm spin}|S,S\rangle\ .$$

Here the states $|M_i,M_j\rangle$ refer to the magnetic quantum numbers ($-\frac{5}{2}\le M_i,M_j\le\frac{5}{2}$) of the Mn spins at $\mathbf{R}_i$ and $\mathbf{R}_j$, $D_\pm(\mathbf{R}_{ij})=D_x(\mathbf{R}_{ij})\pm iD_y(\mathbf{R}_{ij})$, and we have used the antisymmetry of the DM interaction $[D(\mathbf{R}_{ij})=-D(\mathbf{R}_{ij})]$ in obtaining Eq. (2.9). The specification of $|M_i,M_j\rangle$ implicitly includes filled valence bands and empty conduction bands.

Microscopic expressions for the exchange constants are obtained by computing the matrix elements on the right-hand side of Eqs. (2.8) and (2.9) using the more fundamental Hamiltonian H [Eq. (2.1)] in fourth-order perturbation theory. We find (suppressing $\mathbf{R}_{ij}$)

$$-i(\tfrac{5}{2})\sqrt{5}D_+=\sum_{I_1,I_2,I_3}\frac{\langle S-1,S|H_{pd}|I_1\rangle\langle I_1|H_{pd}|I_2\rangle\langle I_2|H_{pd}|I_3\rangle\langle I_3|H_{pd}|S,S\rangle}{(E_0-E_1)(E_0-E_2)(E_0-E_3)}\ , \tag{2.10}$$

$$J+iD_z=-\frac{1}{(2S)}\sum_{K_1,K_2,K_3}\frac{\langle S,S-1|H_{pd}|K_1\rangle\langle K_1|H_{pd}|K_2\rangle\langle K_2|H_{pd}|K_3\rangle\langle K_3|H_{pd}|S-1,S\rangle}{(E_0-E_1^K)(E_0-E_2^K)(E_0-E_3^K)}\ , \tag{2.11}$$

and

$$J-iD_z=-\frac{1}{2S}\sum_{L_1,L_2,L_3}\frac{\langle S-1,S|H_{pd}|L_1\rangle\langle L_1|H_{pd}|L_2\rangle\langle L_2|H_{pd}|L_3\rangle\langle L_3|H_{pd}|S,S-1\rangle}{(E_0-E_1^L)(E_0-E_2^L)(E_0-E_3^L)}\ . \tag{2.12}$$

The intermediate states I_1,I_2,I_3, characterized in Fig. 1, are specified by occupation of *sp*-band states and Mn sites containing four, five, or six electrons. E_0,E_1,E_2,E_3 denote the ground-state and intermediate-state energies, respectively. Because the material is a semiconductor, the energy denominators cannot vanish, and no singularities arise. Figure 1 shows a schematic picture of processes contributing to (a) $J(\mathbf{R}_{ij})$ and (b) $\mathbf{D}(\mathbf{R}_{ij})$. For simplicity the figure is constructed as though $\mathbf{D}(\mathbf{R}_{ij})$ were computed only to first order in λ_a. Our calculation, however, uses valence-band wave functions fully incorporating the mixing due to spin-orbit interactions. The initial- and final-state spin configurations are indicated by solid and dashed arrows, respectively. The total spin in 1(b) decreases by one in going from the initial to the final state, while the total spin in 1(a) is conserved. Figure 1(a) showing processes contributing to isotropic superexchange is equivalent to Fig. 4 of Ref. 8, and is included here only for comparison. The expression for $J(\mathbf{R}_{ij})$, obtained by adding Eqs. (2.11) and (2.12), is equivalent to that of Ref. 8. The only significant contributions are due to the hole intermediate states.

In the first step (A) an electron is transferred from valence-band state $(\mu,\mathbf{k})$ to a spin-down state on $\mathbf{R}_i$ in orbital m creating the intermediate state I_1, with associated energy denominator $\varepsilon_\mu(\mathbf{k})-(\varepsilon_d+U_{\rm eff})$. In step B an electron is transferred from a spin-up state on the Mn ion at $\mathbf{R}_j$ in orbital m' to the valence-band hole at $(\mu,\mathbf{k})$ created in step A. The spin-flip (A') occurs between A and B. The energy denominator associated with B is just $U_{\rm eff}$. Steps C and D, leading to the intermediate state I_3 and the final state, respectively, have the net effect of a spin-parallel transfer of one electron from i back to j. The energy denominator associated with C is $\varepsilon_{\mu'}(\mathbf{k}')-(\varepsilon_d+U_{\rm eff})$. Addition of the six possible processes,[46] summed over d orbitals m,m', and valence bands $(\mu,\mathbf{k}),(\mu',\mathbf{k}')$, and divided by $5^{1/2}$ (from the final-state normalization), leads to

$$\begin{aligned}D_x+iD_y=\tfrac{2}{25}\sum_{m,m'}\sum_{\mu,\mathbf{k}}\sum_{\mu',\mathbf{k}'}&\frac{\sin[(\mathbf{k}-\mathbf{k}')\cdot\mathbf{R}_{ij}]\tilde{V}_{pd}(\mu,\mathbf{k};m,\downarrow)\tilde{V}^*_{pd}(\mu',\mathbf{k}';m,\uparrow)}{[\varepsilon_\mu(\mathbf{k})-(\varepsilon_d+U_{\rm eff})][\varepsilon_{\mu'}(\mathbf{k}')-(\varepsilon_d+U_{\rm eff})]}\\ &\times(\tilde{V}_{pd}(\mu',\mathbf{k}';m',\downarrow)\tilde{V}^*_{pd}(\mu,\mathbf{k};m',\downarrow)\\ &\times\{U_{\rm eff}^{-1}-[\varepsilon_\mu(\mathbf{k})-(\varepsilon_d+U_{\rm eff})]^{-1}-[\varepsilon_{\mu'}(\mathbf{k}')-(\varepsilon_d+U_{\rm eff})]^{-1}\}\\ &-\tilde{V}_{pd}(\mu',\mathbf{k}';m',\uparrow)\tilde{V}^*_{pd}(\mu,\mathbf{k};m',\uparrow)U_{\rm eff}^{-1})\end{aligned} \tag{2.13}$$

and

$$\begin{aligned}J(R_{ij})=-\tfrac{2}{25}\sum_{m,m'}\sum_{\mu,\mathbf{k}}\sum_{\mu',\mathbf{k}'}&\cos[(\mathbf{k}-\mathbf{k}')\cdot\mathbf{R}_{ij}]\frac{\tilde{V}^*_{pd}(\mu,\mathbf{k};m,\uparrow)\tilde{V}_{pd}(\mu,\mathbf{k};m',\uparrow)\tilde{V}^*_{pd}(\mu',\mathbf{k}';m',\downarrow)\tilde{V}_{pd}(\mu',\mathbf{k}';m,\downarrow)}{[\varepsilon_\mu(\mathbf{k})-(\varepsilon_d+U_{\rm eff})][\varepsilon_{\mu'}(\mathbf{k}')-(\varepsilon_d+U_{\rm eff})]}\\ &\times\{U_{\rm eff}^{-1}-[\varepsilon_\mu(\mathbf{k})-(\varepsilon_d+U_{\rm eff})]^{-1}\}\ .\end{aligned} \tag{2.14}$$

Equation (2.14) differs from its counterpart [Eq. (4.4)] in Ref. 8 only in the inclusion of spin-orbit coupling. A perturbative calculation for a simple three-site model[2] shows $D/J\sim\lambda_a/(E_V-\varepsilon_d-U_{\rm eff})$ seen here as the dimensionless factor associated with the wavy line, which expresses the numerical reduction in processes leading to anisotropic relative to isotropic exchange.

B. Results for $Cd_{1-x}Mn_xTe$

The $\mathbf{k}$ sums in Eqs. (2.13) and (2.14) were evaluated using the special-points method of Baldereschi.[20,21,47] Calculations of $J(\mathbf{R}_{ij})$ [Eq. (2.14)] using two special points differed by only $\sim5\%$ from those using the next-larger set of ten points in the irreducible wedge of the first Brillouin zone. The tenpoint calculations, which include the contributions from all plane waves $e^{i\mathbf{k}\cdot\mathbf{R}}$ for $\mathbf{R}$ within the set of the 36 nearest-neighbor shells of direct-lattice vectors, are therefore adequately converged.

The first column of Table I contains the resulting value of J_1 together with input parameters, and the corresponding values obtained from the spherical approximation of Ref. 8, and experiment ($J_1^{\rm expt}$).[8] The experimental exchange constants $J_1^{\rm expt}=-6.3$ K (Ref. 9) and -6.1 K (Ref. 10) are seen to lie between the two theoretical values, which differ by only $\sim25\%$.

The same ten-special-point scheme was used to compute $\mathbf{D}(\mathbf{R}_{ij})$ for NN in $Cd_{1-x}Mn_xTe$. The computed

magnitude of $\mathbf{D}(\mathbf{R}_{ij})=D_1=0.3$ K is shown in the first column of Table I, as is the ratio $|D_1/J_1|=0.05$. D_1 will be seen to dominate other anisotropic coupling mechanisms. The direction of $\mathbf{D}(\mathbf{R}_{ij})$ is determined by symmetry arguments. Evaluation of Eq. (2.13) yields the x and y components of $\mathbf{D}(\mathbf{R}_{ij})$ for a given NN lattice vector $\mathbf{R}_{ij}$. For $\mathbf{R}=(a/2)(1,1,0)$ either component is sufficient to determine $\mathbf{D}((a/2)(1,1,0))$ completely. The remaining component $D_z((a/2)(1,1,0))=0$ can be obtained by exploiting the threefold rotation axis [along (111)] and computing $D_y((a/2)(1,0,1))=D_z((a/2)(1,1,0))=0$. Thus, $\mathbf{D}((a/2)(1,1,0))=2^{-1/2}D_1(\hat{\mathbf{x}}-\hat{\mathbf{y}})$. For a range of compositions $0.1\leq x\leq 0.7$ both J_1 and D_1 increase with x by $\sim 7\%$. The insensitivity to compositional changes reflects the local character of the exchange process.

C. Chemical trends in DM exchange

The same approach was used to calculate J_1 and D_1 for $A^{\mathrm{II}}_{1-x}\mathrm{Mn}_x B^{\mathrm{VI}}$ (A^{II}=Cd,Zn; B^{VI}=Te,Se,S). The sp-band structure was assumed unchanged, but the values of ε_d, U_{eff}, and $N\beta$ were adjusted in accord with the three-level model (Table I).[8] The anion spin-orbit coupling λ_a is taken from tight-binding parametrizations of CdSe and CdS.[22] The hybridization parameters $(pd\sigma)$ and $(pd\pi)$ are determined from the sp-d exchange constants $N\beta$ through Eq. (2.6) as for $\mathrm{Cd}_{1-x}\mathrm{Mn}_x\mathrm{Te}$.

The results for J_1, D_1, $|D_1/J_1|$, and J_1^{expt} are shown in the remaining columns of Table I. The trends in J_1 have already been discussed in Ref. 8. The sign and direction of $\mathbf{D}(\mathbf{R}_{ij})$ in all cases is the same as for $\mathrm{Cd}_{1-x}\mathrm{Mn}_x\mathrm{Te}$.

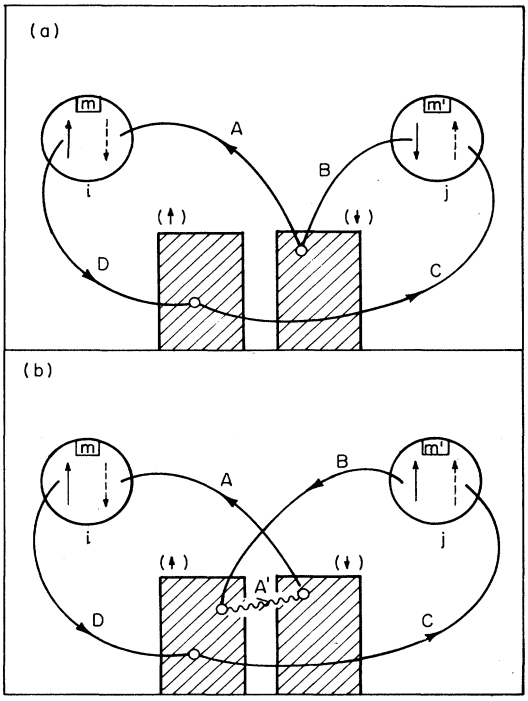

FIG. 1. Schematic representation of terms contributing to (a) $J(\mathbf{R}_{ij})$ and (b) $D_x(\mathbf{R}_{ij})+iD_y(\mathbf{R}_{ij})$ [Eq. (2.13)]. Circles represent d orbitals m at i and m' at j. The initial and final states are indicated by solid and dashed arrows, respectively. Each of the arrows labeled A,B,C,D represents a spin-conserving transfer into or out of valence band states, shown with separate spin components.

TABLE I. Electronic input parameters ($E_V-\varepsilon_d, U_{\mathrm{eff}}, N\beta, \lambda_a$), calculated and experimental nearest-neighbor exchange constants ($J_1, D_1, J_1^{\mathrm{expt}}$), and dipolar coupling constants d_{dip} for $A^{\mathrm{II}}_{0.67}\mathrm{Mn}_{0.33}B^{\mathrm{VI}}$ (A^{II}=Cd,Zn; B^{VI}=Te,Se,S).

		$x=0.33$					
		$\mathrm{Cd}_{1-x}\mathrm{Mn}_x\mathrm{Te}$	$\mathrm{Cd}_{1-x}\mathrm{Mn}_x\mathrm{Se}$	$\mathrm{Cd}_{1-x}\mathrm{Mn}_x\mathrm{S}$	$\mathrm{Zn}_{1-x}\mathrm{Mn}_x\mathrm{Te}$	$\mathrm{Zn}_{1-x}\mathrm{Mn}_x\mathrm{Se}$	$\mathrm{Zn}_{1-x}\mathrm{Mn}_x\mathrm{S}$
Theory							
	$E_V-\varepsilon_d$	3.4[a]	3.4[b]	3.4[c]	3.4	3.4[d]	3.4
Inputs (eV)	U_{eff}	7.0[e]	7.6	7.9	7.0	7.6	7.9
	$N\beta$	−0.88[f]	−1.11[g]	−1.80[h]	−1.05[i]	−1.31[j]	
	λ_a	0.34[k]	0.15[l]	0.023[l]	0.34	0.15	0.023
Outputs (K)	J_1 [spherical; Ref. 8]	−7.6	−9.0	−21.0	−11.0	−13.0	−27.0
	J_1 [sp. points; Eq. (2.14)]	−5.6	−7.3	−17.4	−8.0	−10.1	−22.4
	D_1 [sp. points; Eq. (2.13)]	0.30	0.16	0.055	0.43	0.22	0.07
	$\lvert D_1/J_1\rvert$	0.054	0.022	0.0032	0.054	0.022	0.0031
Expt.		−6.3[m]	−7.9[m]	−8.6[p]	−8.8[q]	−9.9[p]	
					−9.3[r]		−16.1[s]
J_1^{expt}		−6.1[n]	−8.1[o]	−10.6[o]	−9.5[s]	−12.3[s]	
Dipolar coupling (K)							
d_{dip}		0.013	0.016	0.018	0.015	0.019	0.021

[a] Reference 85.
[b] Reference 86.
[c] References 87 and 88.
[d] Reference 89.
[e] Reference 90.
[f] References 45 and 91.
[g] References 92–95.
[h] Reference 96.
[i] References 92, 93, 97, and 98.
[j] References 92, 93, and 99.
[k] Reference 16.
[l] Reference 22.
[m] Reference 9.
[n] Reference 10.
[o] Reference 74.
[p] Reference 100.
[q] Reference 101.
[r] Reference 102.
[s] Reference 103.

However, the magnitudes D_1 decrease with decreasing anion spin-orbit strength λ_a to $D_1=0.055$ K for $Cd_{1-x}Mn_xS$. The calculated cation trends in $D_1 \propto \lambda_a J_1$ can be explained by observing that $|D_1/J_1|$ remains nearly constant for the corresponding Cd- and Zn-based DMS. The independence of $|D_1/J_1|$ on the nonmagnetic cation is consistent with the conclusion, based on the three-level model, that the main effect of substituting Zn for Cd is an increase in the hybridization strength.[8] The hybridization parameters appear as prefactors [Eqs. (2.13) and (2.14)], which effectively cancel in the ratio $|D_1/J_1|$.

The DM interaction is much larger than the two other (dipolar and single-ion) anisotropic terms in the spin Hamiltonian of potential importance. For all the Mn-based DMS considered here, the magnitude of the dipolar coupling, $d_{\rm dip} \equiv \frac{1}{2} r_{\rm NN}^{-3} (g\mu_B)^2$, is less than 20 mK for NN distances.[49] (Here $r_{\rm NN}$ is the separation of nearest magnetic neighbors.) For the uniaxially symmetric z-oriented wurtzite DMS ($Cd_{1-x}Mn_xSe$, $Cd_{1-x}Mn_xS$, $Zn_{1-x}Mn_xS$) the appropriate single-ion term $H_{\rm uniaxial}$ has the form $D_{\rm single} \sum_i' S_{iz}^2$. In wurtzite DMS $D_{\rm single}$ is found to be positive (an *easy plane* situation) and ≤ 40 mK.[50–52] For cubic symmetry ($Cd_{1-x}Mn_xTe$, $Zn_{1-x}Mn_xTe$) the lowest-order term $H_{\rm cubic}$ is[24] $-(a_{\rm cub}/6)\sum_i' (S_{ix}^4+S_{iy}^4+S_{iz}^4)$. In $Cd_{1-x}Mn_xTe$ and $Zn_{1-x}Mn_xTe$, $a_{\rm cub} \sim 5$ mK.[50–52] We shall regard $D_{\rm single}$ and $a_{\rm cub}$ as phenomenological parameters since they are relatively unimportant.

III. EPR LINEWIDTHS

A. EPR experiments on DMS

In the absence of measurements on isolated spin pairs, EPR offers the best opportunity to determine D_1. Anisotropic exchange breaks the conservation of total magnetization implied by isotropic exchange and broadens the line significantly by suppressing exchange narrowing.

To see how this occurs, consider the spin Hamiltonian

$$\tilde{H}(t) = -\sum_{i \neq j} J(R_{ij}) \mathbf{S}_i \cdot \mathbf{S}_j - \mathcal{M} \cdot \mathbf{H}(t) \ , \tag{3.1}$$

where $\mathbf{H}(t)=H_0\hat{\mathbf{z}}+\mathbf{H}_1(t)$, $\mathbf{H}_1(t)=H_1(t)\hat{\mathbf{x}}$ is the oscillating field, and $H_1 \ll H_0$. The Heisenberg equation of motion for the x component of the magnetization $\mathcal{M}_x(t)$ is

$$i\hbar\dot{\mathcal{M}}_x = [\mathcal{M}_x, \tilde{H}] \quad \text{with } \mathcal{M}_x \equiv g\mu_B \sum_i' S_{ix} \ . \tag{3.2}$$

Dots denote time derivatives and primed sums indicate that only Mn-occupied sites are included. When the Hamiltonian of Eq. (3.1) is substituted into Eq. (3.2), the commutator arising from the exchange term vanishes, reflecting spin conservation. The remaining term,

$$\dot{\mathcal{M}}_x(t) = \frac{g\mu_B}{\hbar} [\mathcal{M}(t) \times \mathbf{H}(t)]_x \ ,$$

describes Larmor precession at frequency $\omega_0 \equiv g\mu_B H_0/\hbar$ for $H_1=0$. Anisotropic terms in the spin Hamiltonian are required to obtain a nonvanishing linewidth. The most important of these for $Cd_{1-x}Mn_xTe$ is the DM exchange.

EPR experiments on concentrated DMS have focused on temperatures just above $T_{\rm SG}$, the spin-glass transition.[26,27,35,36,53–57] We consider only the higher-temperature linewidths measured as a by-product. All DMS studied so far exhibit these following qualitative features. (1) The line broadens dramatically with decreasing temperature T and with increasing concentration x. (2) The line shape is Lorentzian. (3) At fixed $T \gg 20$ K for $x \geq 0.1$ the linewidth for a given nonmagnetic cation (Cd or Zn) decreases as the anion is changed in the order Te,Se,S.[26,27] The experimental temperature dependence of the linewidth is fit acceptably by various phenomenological formulas.[1,27,35,36,53–57]

Experimental high-temperature EPR data is usually fit to an expression for the line shape derived from the Bloch equation[24]

$$\dot{\mathcal{M}} = \frac{g\mu_B}{\hbar} \mathcal{M} \times \mathbf{H}(t) - \tau^{-1} [\mathcal{M} - \chi_0 \mathbf{H}(t)] \ , \tag{3.3}$$

modified for the case where the longitudinal (energy) and transverse (angular momentum) relaxation times are equal: $T_1=T_2=\tau$. Equation (3.3) is valid within the relaxation time approximation: $\omega\tau \ll 1$.[24,26,27] This limit is appropriate to the broad resonances observed in DMS,[26,27] where typically $\tau \sim 10^{-10}$ sec, whereas $\omega \sim 10^9$–10^{10} Hz.

B. Microscopic response-function moments

We calculate the EPR linewidth using the linear-response-function formalism.[58,59] For a cubic crystal or isotropic powder sample the absorptive and complex responses to the magnetic field $\mathbf{H}_1(\omega) = \int_{-\infty}^{\infty} e^{i\omega t} \mathbf{H}_1(t) dt$ are given by

$$\chi''(\omega) = \frac{1}{2\hbar} \int_{-\infty}^{\infty} e^{i\omega t} \langle [\mathcal{M}_x(t), \mathcal{M}_x(0)] \rangle dt \ , \tag{3.4}$$

$$\chi(z) = \int_{-\infty}^{\infty} \frac{d\omega}{\pi} \frac{\chi''(\omega)}{\omega - z} \quad (\mathrm{Im} z \neq 0) \ . \tag{3.5}$$

The memory function[60,61] is

$$\Delta(z) = \frac{z\chi(z)}{\chi(z) - \chi_0} \ . \tag{3.6}$$

The EPR line-shape function is

$$I(\omega) = \frac{\chi''(\omega)}{\omega\chi_0} = \frac{\Delta''(\omega)}{[\omega - \Delta'(\omega)]^2 + [\Delta''(\omega)]^2} \ , \tag{3.7}$$

where χ_0 is the static susceptibility. In the relaxation-time approximation $\Delta''(\omega)=\tau^{-1}$ and $\Delta'(\omega)=\omega_0$. This equation defining the line shape $I(\omega)$ is central to our discussion. Clearly the line will be approximately Lorentzian when $\Delta'(\omega)$ and $\Delta''(\omega)$, the real and imaginary parts of the memory function, are nearly constant over the width of the Lorentzian. The Larmor frequency ω_0 is sufficiently small compared to J_1 that to good approximation the linewidth is unchanged from its zero-field value ($\omega_0=0$), which we calculate.

We shall determine $\Delta''(\omega)$ from a set of its frequency

moments L_n, and related response-function moments M_n, defined, respectively, by

$$L_n \equiv \int_{-\infty}^{\infty} \frac{d\omega}{\pi} \omega^n \Delta''(\omega) , \tag{3.8}$$

$$M_n \equiv \int_{-\infty}^{\infty} \frac{d\omega}{\pi} \omega^{n-1} \frac{\chi''(\omega)}{\chi_0} = \int_{-\infty}^{\infty} \frac{d\omega}{\pi} \omega^n I(\omega) . \tag{3.9}$$

M_n and L_n vanish if n is odd.[62] The two sets of moments are related by

$$L_0 = M_2, \quad L_2 = M_4 - M_2^2, \ldots .$$

The spin Hamiltonian

$$H_{\text{spin}} = H_H + H_{\text{DM}} + H_{\text{dip}} + H_{\text{single}} \tag{3.10}$$

for computing the moments is the sum of the terms discussed in Sec. II.

We ignore the small H_{single} for the present, but will reconsider its effects in Sec. III D. The explicit form of H_{spin} restricted to nearest neighbors is then

$$H_{\text{spin}} = -\sum_{\substack{i \neq j \\ (\text{NN})}}{}' \{ J_1 \mathbf{S}_i \cdot \mathbf{S}_j + \mathbf{D}_1(\hat{\mathbf{r}}_{ij}) \cdot \mathbf{S}_i \times \mathbf{S}_j - d_{\text{dip}} [\mathbf{S}_i \cdot \mathbf{S}_j - 3(\mathbf{S}_i \cdot \hat{\mathbf{r}}_{ij})(\mathbf{S}_j \cdot \hat{\mathbf{r}}_{ij})] \} . \tag{3.11}$$

Here $\hat{\mathbf{r}}_{ij}$ are the unit vectors to the 12 nearest-neighbor (NN) magnetic-lattice sites, and $\mathbf{D}_1(\hat{\mathbf{r}}_{ij}) = \mathbf{D}(\mathbf{R}_{ij})$ for NN $\mathbf{R}_{ij}$.

The equality between Eqs. (3.11) and (1.1) defines the $\mathcal{J}_{\mu\nu}(\hat{\mathbf{r}}_{ij})$ introduced in Sec. I. We introduce the site occupation variables ξ_i corresponding magnetic lattice site $\mathbf{R}_i$: $\xi_i = 1$ and 0 for Mn-occupied sites having spin $\mathbf{S}_i$ and unoccupied sites, respectively. Thus

$$H_{\text{spin}} = -\sum_{\substack{i \neq j \\ (\text{NN})}} S_{i\mu} \mathcal{J}_{\mu\nu}(\hat{\mathbf{r}}_{ij}) S_{j\nu} \xi_i \xi_j . \tag{3.12}$$

At experimental temperatures ($T_{\text{SG}} \ll T \leq 300$ K) the values of the ξ_i are effectively frozen and hence not included in the thermal averaging represented below by angle brackets. The ξ_i are averaged over in a subsequent step, assuming (1) that occupations of different sites are completely independent, and (2) that $\xi_i = 1$ with probability x, while $\xi_i = 0$ with probability $1-x$. The absence of nonstatistical clustering is experimentally verified for $x \leq 0.05$ DMS.[63]

We now derive explicit expressions for M_2 and M_4 from Eqs. (3.9) and (3.4) to $O(T^{-1})$ in a high-temperature expansion. By converting the powers of ω to time derivatives acting on the Fourier transform, integrating by parts, and using Eq. (3.2) for $\mathcal{M}_x(t)$, we find

$$M_2(T) = -(\hbar^2 \chi_0)^{-1} \langle [[H_{\text{spin}}, \mathcal{M}_x(0)], \mathcal{M}_x(0)] \rangle , \tag{3.13}$$

$$M_4(T) = -(\hbar^4 \chi_0)^{-1} \langle [[H_{\text{spin}}, [H_{\text{spin}}, [H_{\text{spin}}, \mathcal{M}_x(0)]]], \mathcal{M}_x(0)] \rangle . \tag{3.14}$$

Evaluation of higher M_n involves an unacceptable level of complexity given the experimental data presently available.

The static susceptibility has the well-known expansion

$$\chi_0(T) = \tfrac{1}{3} N (k_B T)^{-1} S(S+1) \left[1 - \frac{\Theta_p}{T} + O(T^{-2}) \right] . \tag{3.15}$$

Here N is the number of spins, $S = \frac{5}{2}$, and Θ_p is the paramagnetic Curie temperature,[64]

$$\Theta_p \equiv \frac{\text{Tr}(H_{\text{spin}} \mathcal{M}_x^2)}{\text{Tr}(\mathcal{M}_x^2)} = -\tfrac{2}{3} S(S+1) \sum_{i(\text{NN})} \mathcal{J}_{xx}(\mathbf{R}_i) \xi_i . \tag{3.16}$$

Denoting averages over the ξ_i by a bar with $\bar{\xi}_i = x$, and recalling that $J_1 \gg D_1$, or d_{dip}, we find

$$\bar{\Theta}_p \approx -\tfrac{2}{3} S(S+1) J_1 z_1 x + O(D_1) .$$

Here the coordination number $z_1 = 12$ is the number of nearest neighbors on the fcc magnetic lattice. Expansion of the thermal averages in Eqs. (3.13) and (3.14), use of the cyclic invariance of the trace, and substitution of the expansion (3.15) for $\chi_0(T)$ yields

$$M_n(T) = M_n^{\infty} \left[1 + \frac{\Theta_p + \Theta_n}{T} + O(T^{-2}) \right] \quad (n = 2, 4) , \tag{3.17}$$

a result which is central to the subsequent discussion. The terms in Eq. (3.17) have the definitions

$$M_2^{\infty} = \frac{-\text{Tr}([\hbar^{-1} H_{\text{spin}}, \mathcal{M}_x]^2)}{\text{Tr}\mathcal{M}_x^2} = \frac{\text{Tr}\dot{\mathcal{M}}_x^2}{\text{Tr}\mathcal{M}_x^2} , \tag{3.18}$$

$$M_4^{\infty} = \frac{\text{Tr}([\hbar^{-1} H_{\text{spin}}, [\hbar^{-1} H_{\text{spin}}, \mathcal{M}_x]]^2)}{\text{Tr}\mathcal{M}_x^2} = \frac{\text{Tr}\ddot{\mathcal{M}}_x^2}{\text{Tr}\mathcal{M}_x^2} , \tag{3.19}$$

$$k_B \Theta_2 = -\frac{1}{2} \frac{\text{Tr}(H_{\text{spin}} [\hbar^{-1} H_{\text{spin}}, \mathcal{M}_x]^2)}{\text{Tr}([\hbar^{-1} H_{\text{spin}}, \mathcal{M}_x]^2)} = -\frac{1}{2} \frac{\text{Tr}(H_{\text{spin}} \ddot{\mathcal{M}}_x^2)}{\text{Tr}\dot{\mathcal{M}}_x^2} , \tag{3.20}$$

$$k_B\Theta_4=-\frac{1}{2}\frac{\mathrm{Tr}(H_{\mathrm{spin}}[\hbar^{-1}H_{\mathrm{spin}},[\hbar^{-1}H_{\mathrm{spin}},\mathcal{M}_x]]^2)}{\mathrm{Tr}([\hbar^{-1}H_{\mathrm{spin}},[\hbar^{-1}H_{\mathrm{spin}},\mathcal{M}_x]]^2)}$$
$$=-\frac{1}{2}\frac{\mathrm{Tr}(H_{\mathrm{spin}}\ddot{\mathcal{M}}_x^2)}{\mathrm{Tr}\ddot{\mathcal{M}}_x^2}\ . \tag{3.21}$$

The final equality in each of Eqs. (3.18)–(3.21) follows from the Heisenberg equation of motion for $\mathcal{M}_x(t)$ (for M_2^∞,Θ_2) or $\dot{\mathcal{M}}_x(t)$ (for M_4^∞,Θ_4). Although the thermodynamic averaging is implied by the traces, these expressions still implicitly depend on the site occupations ξ_i ($i=1,2,\ldots,N$), which remain to be averaged.

Equations (3.18) and (3.19) have been derived and evaluated for $H_{\mathrm{spin}}=H_H+H_{\mathrm{dip}}$ by Van Vleck.[25] The expressions for Θ_2 and Θ_4 are new, as is the calculation of M_4^∞ for the more-general spin Hamiltonian of Eq. (3.10).

Simple estimates providing physical insight concerning moments, linewidths, and exchange narrowing can be obtained by ignoring H_{dip}. Equation (3.2) then yields

$$i\hbar\dot{\mathcal{M}}_x=[\mathcal{M}_x,H_H]+[\mathcal{M}_x,H_{\mathrm{DM}}]\approx D_1\mathcal{M}_x \tag{3.22}$$

because $[\mathcal{M}_x,H_H]=0$. Substituting Eq. (3.22) into Eq. (3.18) shows

$$M_2^\infty=\frac{\mathrm{Tr}\dot{\mathcal{M}}_x^2}{\mathrm{Tr}\mathcal{M}_x^2}\approx\frac{\mathrm{Tr}(D_1\mathcal{M}_x/i\hbar)^2}{\mathrm{Tr}\mathcal{M}_x^2}\sim(D_1/\hbar)^2 \tag{3.23}$$

to be *independent of the strength of the isotropic exchange* J_1.[25]

To estimate M_4^∞ we need the Heisenberg equation for $\dot{\mathcal{M}}_x(t)$:

$$i\hbar\ddot{\mathcal{M}}_x=[\dot{\mathcal{M}}_x,H_H]+[\dot{\mathcal{M}}_x,H_{\mathrm{DM}}]\approx J_1\dot{\mathcal{M}}_x\sim J_1D_1\mathcal{M}_x/\hbar\ , \tag{3.24}$$

since $[\dot{\mathcal{M}}_x,H_H]$ does not vanish. Substitution into Eq. (3.19) yields

$$M_4^\infty=\frac{\mathrm{Tr}\ddot{\mathcal{M}}_x^2}{\mathrm{Tr}\mathcal{M}_x^2}\approx\frac{\mathrm{Tr}[J_1D_1\mathcal{M}_x/(i\hbar)^2]^2}{\mathrm{Tr}\mathcal{M}_x^2}\sim\frac{J_1^2D_1^2}{\hbar^4}\ . \tag{3.25}$$

The coefficients Θ_2 and Θ_4 are seen to be $O(J_1)$ when $J_1\gg D_1$. This follows from Eqs. (3.20), (3.21), and the fact that J_1 is the dominant energy parameter in H_{spin}. D_1 is the dominant energy in the opposite limit, $J_1\ll D_1$. Then $M_n^\infty\sim(D_1/\hbar)^n$ for $n=2,4$, consistent with a Gaussian line. By contrast, a (cutoff) Lorentzian line shape *can* be obtained when $J_1\gg D_1$, the case of interest, because $M_4^\infty\gg(M_2^\infty)^2$.

C. Maximum-entropy method and exchange narrowing

The maximum-entropy method[30–33,65–68] will be used to obtain $\Delta''(\omega)$ and thereby $I(\omega)$. Let $P(\omega)=(\pi L_0)^{-1}\Delta''(\omega)$ be a probability density, normalized by the definition of L_0 [Eq. (3.8)]. The second moment of $P(\omega)$ is just L_2/L_0. The function $P(\omega)$ is obtained by demanding that it correspond to the maximum of an information theoretic entropy $S[P]$ defined by

$$S[P]=-\int_{-\infty}^{\infty}[P(\omega)\ln P(\omega)-P(\omega)]d\omega\ .$$

A variational calculation incorporating the two known moments as constraints through appropriate Lagrange multipliers yields

$$P(\omega)=(\pi L_0^{-1})\Delta''(\omega)=e^{-\lambda_0}e^{-\lambda_2\omega^2}\ .$$

The Lagrange multipliers λ_0 and λ_2 are determined analytically from the normalization and second moment of $P(\omega)$. The resulting memory-function imaginary part

$$\Delta''(\omega)=\pi L_0P(\omega)=\left[\frac{\pi L_0^3}{2L_2}\right]^{1/2}e^{-L_0\omega^2/2L_2} \tag{3.26}$$

is seen to be Gaussian.[69] $\Delta'(\omega)$ is obtained as a Kramers-Kronig transform:

$$\Delta'(\omega)=\Delta''(\omega)\frac{2}{\sqrt{\pi}}\int_0^{\omega(L_0/2L_2)^{1/2}}e^{t^2}dt\ . \tag{3.27}$$

The interpretation of $P(\omega)$ as a probability follows from the fact that $\Delta''(\omega)$ is a spectral density associated with an elementary excitation. Here the excitations correspond to modes of the system through which $\partial_t\mathcal{M}_x$ relaxes.[70]

Exchange narrowing may be understood on a qualitative physical basis with the help of Eqs. (3.26), (3.27), and the moment estimates (3.23). For $J_1\gg D_1$, the memory-function moments L_0 and L_2 are approximately equal to M_2^∞ and M_4^∞, respectively. Let

$$\omega_e^2\equiv\frac{2L_2}{L_0}\sim\frac{M_4}{M_2}\sim\left[\frac{J_1}{\hbar}\right]^2 \tag{3.28}$$

define an exchange frequency. Then

$$\Delta''(\omega)=\frac{\sqrt{\pi}L_0}{\omega_e}e^{-(\omega/\omega_e)^2}\approx\frac{D_1^2}{\hbar J_1}e^{-(\omega/\omega_e)^2} \tag{3.29}$$

is nearly constant for $\omega\ll\omega_e$. Since $\Delta'(0)=0$, Eq. (3.27) ensures $\Delta'\ll\omega$ for $\omega\ll\omega_e$. Thus $I(\omega)$, given by Eq. (3.7) is Lorentzian for $\omega\ll\omega_e$, with linewidth $\sim D_1^2/J_1$.[71] The Gaussian decay of $\Delta''(\omega)$ becomes important only for $\omega\sim\omega_e$, where $I(\omega)\ll I(0)$.[72]

The exchange-narrowing process may be understood by comparing this result with that for the opposite limit $J_1\ll D_1$, where the linewidth is of order D_1. If the value of J_1 were increased from $J_1\ll D_1$ to $J_1\gg D_1$, the linewidth, having initial width $\sim D_1$, would decrease to D_1^2/J_1.

The theory of Anderson and Weiss and the similar approach of Kubo and Tomita are also based on evaluating M_2 and M_4, but treat exchange narrowing in terms of a random modulation with time of the local fields.[28] The numerical linewidths obtained in Sec. III D were duplicated to $\sim3\%$ using the same moments and the Anderson-Weiss theory.

D. Calculation of the linewidths for DMS

The moments M_2^∞ and M_4^∞ and the temperatures Θ_2 and Θ_p, given by Eqs. (3.18), (3.19), (3.20), and (3.16) are calculated as follows. (1) M_4^∞ is simplified by the approximation[25] $[H_{\mathrm{spin}},[H_{\mathrm{spin}},\mathcal{M}_x]]\approx[H_H,[H_{\mathrm{spin}},\mathcal{M}_x]]$

$+O(D_1^2\mathcal{M}_x)$. (2) The traces are carried out in a basis of spin eigenstates.[2] (3) All realizations of the site occupation variables are averaged.[73]

$\overline{M}_2^{\infty}$ is given by the sum

$$\overline{M}_2^{\infty}=\tfrac{1}{3}S(S+1)x \times \sum_{\mathbf{R}_i}^{(\mathrm{NN})} \sum_{\alpha,\beta} \sum_{\mu,\nu} [\varepsilon_{\mu x\beta} I_{\alpha\mu}(\mathbf{R}_i)+\varepsilon_{\mu x\alpha} I_{\mu\beta}(\mathbf{R}_i)] \times [\varepsilon_{\nu x\beta} I^S_{\alpha\nu}(\mathbf{R}_i)+\varepsilon_{\nu x\alpha} I^S_{\nu\beta}(\mathbf{R}_i)] , \tag{3.30}$$

where

$$I_{\mu\nu}(\mathbf{R}_i)\equiv \mathcal{J}_{\mu\nu}(\mathbf{R}_i)-\tfrac{1}{3}\delta_{\mu\nu}\sum_{\alpha}\mathcal{J}_{\alpha\alpha}(\mathbf{R}_i) ,$$

and

$$I^S_{\mu\nu}(\mathbf{R}_i)=I_{\mu\nu}(\mathbf{R}_i)+I_{\nu\mu}(-\mathbf{R}_i) .$$

Explicit expressions for $\overline{M}_4^{\infty}$ and $\overline{\Theta}_2$ have been given elsewhere.[2] $\overline{M}_4^{\infty}$ contains terms proportional to x and to x^2, while $\overline{\Theta}_2 \propto x$. The remaining sums over lattice sites [as in Eq. (3.30)] were performed numerically. The $\mathcal{J}_{\mu\nu}(\mathbf{R}_{ij})$ for tellurides and selenides were determined from the J_1 and D_1 values calculated in Sec. II. For $Cd_{1-x}Mn_xS$, we used the experimental value $J_1^{\mathrm{expt}}=-10.6$ K (Ref. 74) (Table I) to obtain a value of D_1 using the *calculated* $|D_1/J_1|$ ratio, yielding $D_1=|D_1/J_1|J_1^{\mathrm{expt}}=0.034$ K. The dipolar coupling constants J_{dip} listed in Table I were computed from the lattice constants as a function of x measured for each DMS.[75]

1. *Infinite-temperature linewidth calculations*

The EPR linewidth ΔH_{∞} defined as the full width at half maximum of $I(\omega)$, is calculated from Eq. (3.7), with $\Delta''(\omega)$ and $\Delta'(\omega)$ determined by the calculated $\overline{M}_2^{\infty}$ and $\overline{M}_4^{\infty}$ through Eqs. (3.26) and (3.27). Table II shows the resulting theoretical ΔH_{∞} contributions for $Cd_{1-x}Mn_xTe$, $Cd_{1-x}Mn_xSe$, and $Cd_{1-x}Mn_xS$ (all for $x=0.33$) compared with the infinite temperature extrapolation (discussed below), $\Delta H_{\infty}^{\mathrm{par}}$, of the EPR linewidth data of Samarth and Furdyna.[27] The trends for $x=0.33$ are characteristic of those obtained for other concentrations.

The first three lines show the computed ΔH_{∞} for dipolar, DM, and combined dipolar and DM anisotropic exchange interactions, respectively. The DM contribution is seen to be consistent with the extrapolated experimental trend. By contrast, the dipolar linewidths are far too small compared to experiment and do not exhibit the correct trend. For the sulfide, the contributions of dipolar and DM to ΔH_{∞} are about equal due to weak spin orbit coupling.

The linewidths incorporating both types of anisotropic couplings in line 3 using Eq. (3.7) are nearly the same as the sum of the contributions computed separately. The predicted ratio of $Cd_{1-x}Mn_xTe$ to $Cd_{1-x}Mn_xS$ linewidths is ~ 25, a factor of 2 larger than experiment.[27] The magnitude of ΔH_{∞} in $Cd_{1-x}Mn_xTe$, 603 G, is in good agreement with the extrapolated experimental value (550 G). However, in the selenide and sulfide the predicted linewidths are too small by a factor of 2.

To account for this difference, we have estimated linewidth corrections $\delta\Delta H_{\infty}$ due to single-ion anisotropies (line four), and DM exchange arising from Mn spin-orbit interactions (line 5), as follows.

We take $H_{\mathrm{spin}}=H_H+H_{\mathrm{DM}}+H_{\mathrm{dip}}+H_{\mathrm{single}}$ as in Eq. (3.10), with $J_1 \gg D_1 \gg D_A > d_{\mathrm{dip}}$. Let D_A represent D_{single} or a_{cub} for wurtzite and zinc-blende DMS, respectively. To estimate ΔH_{∞} we repeat the arguments of Eqs. (3.28), (3.29), and the text following (3.29) for this Hamiltonian, to find

$$\Delta H_{\infty} \sim J_1^{-1}(D_1+d_{\mathrm{dip}}+D_A)^2 \sim J_1^{-1}D_1^2+2J_1^{-1}D_1D_A . \tag{3.31}$$

Here terms smaller by factors of D_A/D_1 and d_{dip}/D_A have been neglected. The first term in Eq. (3.31) is the es-

TABLE II. Calculated theoretical and extrapolated experimental infinite-temperature linewidths ΔH_{∞} for $Cd_{0.67}Mn_{0.33}B^{VI}$ (B^{VI}=Te,Se,S) (in G).

		$x=0.33$		
		$Cd_{1-x}Mn_xTe$	$Cd_{1-x}Mn_xSe$	$Cd_{1-x}Mn_xS$
Theory				
	(dipolar only)	11	13	12
ΔH_{∞} (G)	(DM only)	591	127	12
Eq. (3.7)	(dipolar and DM)	603	139	25
	single ion	~ 16	~ 50	~ 8
$\delta\Delta H_{\infty}$ (G)	[Eq. (3.34)]			
	Mn-associated DM	~ 34	~ 20	~ 30
	[Eq. (3.35)]			
Total $\Delta H_{\infty}^{\mathrm{cal}}$ (G)		653	209	63
Expt.				
$\Delta H_{\infty}^{\mathrm{par}}$ (G)		550[a]±200	350[a]±120	40[a]±27
[see Eq. (3.37)]				

[a] Reference 27.

timated linewidth for $D_A = d_{\rm dip} = 0$. Hence,

$$\delta\Delta H_\infty \sim 2D_1 D_A J_1^{-1} \ . \tag{3.32}$$

To make numerical estimates of $\delta\Delta H_\infty$ we assume that the *calculated* ΔH_∞ in line 2 of Table II is proportional to the estimated linewidth,

$$\Delta H_\infty = K D_1^2 J_1^{-1} \ , \tag{3.33}$$

where K is a constant. We find $K \approx 6$ for all DMS. Applying the same proportionality constant to $\delta\Delta H_\infty$ in Eq. (3.32) yields

$$\delta\Delta H_\infty = 2K D_1 D_A J_1^{-1} \ , \tag{3.34}$$

given in line 4 of Table II. The corrections are seen to be ~ 20–30% for the selenide and the sulfide, but negligible for the (zinc-blende) tellurides due to the small size of $a_{\rm cub}$.

The Mn spin-orbit interaction produces an additional DM coupling D_1', which must be added to the anion-associated D_1. The Mn-associated DM exchange vector $\mathbf{D}'(\mathbf{R}_{ij})$ is directed along the same symmetry-determined axis as $\mathbf{D}(\mathbf{R}_{ij})$. Assuming that $\mathbf{D}(\mathbf{R}_{ij})$ and $\mathbf{D}'(\mathbf{R}_{ij})$ have the same sign, the linewidth has the approximate value $\Delta H_\infty = K J_1^{-1}(D_1 + D_1')^2$. The correction to the linewidth $\delta\Delta H_\infty$ due to D_1' is identified by comparing this equation with Eq. (3.33),

$$\delta\Delta H_\infty = K D_1^2 J_1^{-1} \left[\left[1 + \frac{D_1'}{D_1} \right]^2 - 1 \right] . \tag{3.35}$$

Finally, the Mn-associated D_1' is estimated using Moriya's expression[4] $D_1' J_1^{-1} \sim g^{-1} \Delta g$, where $\Delta g \equiv g - 2.0023$. The values of Δg measured in $x < 0.01$ EPR for DMS selenides and sulfides are $(1.5$–$3) \times 10^{-3}$.[50,52] In $Cd_{1-x}Mn_xTe$ and $Zn_{1-x}Mn_xTe$, $\Delta g \sim 5 \times 10^{-1}$.[50,51] We adopt the approximate value $\Delta g = 3 \times 10^{-3}$ for all DMS.

The $\delta\Delta H_\infty$ calculated from Eq. (3.35) are given in line 5 of Table II. In view of the small anion spin-orbit interactions in the sulfide, the effects of Mn spin-orbit interactions are very significant, accounting for $\sim 50\%$ of the total linewidth. By contrast, in the selenide and tellurides, these corrections are only $\sim 10\%$ of the total linewidth.

The total calculated infinite-temperature linewidth ΔH_∞ (the sum of entries in lines 3–5) is given in line 6. The agreement with the extrapolated experimental linewidths is noticeably improved by the two corrections.[76] Clearly DM exchange, including both anion- and Mn-based sources, accounts quantitatively for the majority of the broadening in these DMS.

We expect that the error in the calculated linewidth for $Cd_{1-x}Mn_xTe$ is roughly 30% (Ref. 2) based on the estimated theoretical error in the input exchange constants and results of previous linewidth calculations.[29,77,78] [The error for selenides and sulfides is larger ($\sim 40\%$) because of the importance of the corrections $\delta\Delta H_\infty$.] The smallness of the corrections $\delta\Delta H_\infty$ for $Cd_{1-x}Mn_xTe$ ($\sim 8\%$ of ΔH_∞) leads to a value of D_1 that is accurate to $\sim 20\%$.

2. *Determination of D_1 from finite-temperature linewidth*

Using Eqs. (3.17) for $M_2(T)$ and $M_4(T)$, and Eq. (3.26) for $\Delta''(\omega)$ we define the theoretical high-temperature linewidth $\Delta H(T)$

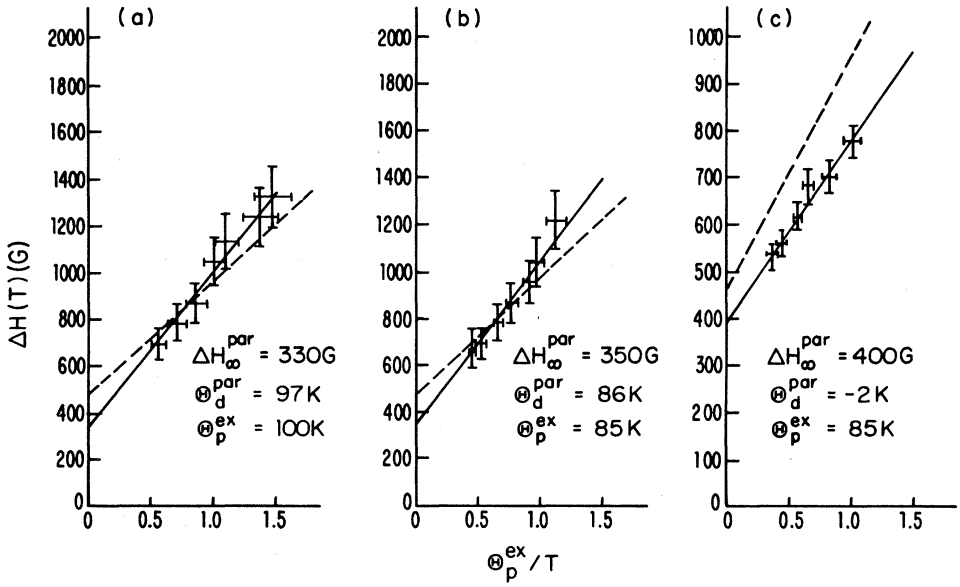

FIG. 2. Experimental data, parametrized fit [solid line, Eq. (3.37)], and theoretical [dashed line, Eq. (3.36)] linewidths for $Cd_{0.80}Mn_{0.20}Te$ as a function of Θ_p^{ex}/T. The points are experimental data of (a) Oseroff (Ref. 35), (b) Sayad and Bhagat (Ref. 36), and (c) Samarth and Furdyna (Ref. 27; different scale).

$$\Delta H(T)=\Delta H_\infty\left[1+\frac{\Theta_p+\Theta_2+\frac{1}{2}(\Theta_2-\Theta_4)}{T}\right] \quad (3.36)$$

to order T^{-1}. Theoretical analysis[2] suggests that the numerator of the temperature-dependent term in Eq. (3.36) is not well-represented numerically by the limited number of moments, Θ_2 and Θ_4, under consideration. This implies that a parametrized form of that equation,

$$\Delta H(T)=\Delta H_\infty^{\rm par}\left[1+\frac{\Theta_p^{\rm ex}+\Theta_d^{\rm par}}{T}\right], \quad (3.37)$$

having the same analytic form will yield a more reliable value of D_1. Here $\Theta_p^{\rm ex}$ is to be taken as the experimental paramagnetic Curie temperature,[79] and $\frac{3}{2}\Theta_2-\frac{1}{2}\Theta_4$ and ΔH_∞ are to be replaced by $\Theta_d^{\rm par}$ and $\Delta H_\infty^{\rm par}$, respectively. The parameters $\Delta H_\infty^{\rm par}$ and $\Theta_d^{\rm par}$ are determined by a least-squares[80] fit of a straight line to $\Delta H(T)$ versus $\Theta_p^{\rm ex}/T$.[81]

The solid lines in Fig. 2 show the results of the fitting procedure for $x=0.20$ data of three experimental groups.[27,35,36] For all concentrations studied, the data is well fit by a straight line. There is no evidence for $O(T^{-2})$ terms, even down to temperatures $\sim\Theta_p^{\rm ex}$. To determine $D_1^{\rm par}$ we fix J_1 at its experimental value (-6.3 K), thereby making D_1 the only undetermined parameter in the expression for ΔH_∞ following from Eq. (3.7), and require the latter to agree with $\Delta H_\infty^{\rm par}$. The resulting $D_1^{\rm par}$ values exhibit significantly increased scatter for $x>0.25$. The average for all $D_1^{\rm par}$ values with $x\le 0.25$ is 0.28 ± 0.01 K, while the average is 0.29 ± 0.07 K for $x>0.25$ (Ref. 82). The scatter may well be associated with the quality of the samples at large x. The majority of the experimental results pertain to small concentrations. The average value is $(D_1^{\rm par})_{\rm av}=0.28\pm0.03$ K.[2] This is the first value of D_1 reported for any DMS. The agreement with the calculated theoretical value $D_1=0.30$ K (Table I) is remarkable, and emphasizes the accuracy and consistency of our theoretical framework.

It is of interest to compare the results of the theoretical expression Eq. (3.36), particularly since Θ_d is expected to be small relative to Θ_p.[2] The result, shown by the dashed lines in Fig. 2 is obtained using the approximation $\Theta_4\sim\Theta_2$ as given by Eq. (3.20). The slopes agree quite well with those obtained from the parametrized fit to experiment because both are dominated by $\Theta_p^{\rm ex}$. This novel analysis therefore establishes the credibility of Eq. (3.37) and its use in determining reliable values of D_1.

ACKNOWLEDGMENTS

The authors wish to thank N. Samarth, J. K. Furdyna, P. A. Fedders, and C. Henley for useful discussions. This research was supported by the U.S. Defense Advanced Research Projects Agency (DARPA) under the Office of Naval Research–Universites Research Initiative (ONR/URI) Contract No. N00014-86-K-0760.

[1]For a recent review including EPR in DMS, see S. Oseroff and P. H. Keesom, in *Diluted Magnetic Semiconductors*, Vol. 25 of *Semiconductors and Semimetals*, edited by J. K. Furdyna and J. Kossut (Academic, New York, 1987).

[2]More detailed descriptions of the calculations presented in this paper are given in B. E. Larson, Ph.D. thesis, Harvard University, 1988.

[3]P. W. Anderson, in *Solid State Physics*, edited by F. Seitz and D. Turnbull (Academic, New Yok, 1963), Vol. 14, p. 99.

[4]T. Moriya, Phys. Rev. **120**, 91 (1960).

[5]I. Dzyaloshinsky, Phys. Chem. Solids **4**, 241 (1958).

[6]The possibility of an antisymmetric exchange term in the spin Hamiltonian was first suggested by K. W. H. Stevens, Rev. Mod. Phys. **25**, 166 (1953).

[7]T. Moriya, in *Magnetism*, edited by G. T. Rado and H. Suhl (Academic, New York, 1963), Vol. 1, p. 85.

[8]B. E. Larson, K. C. Hass, H. Ehrenreich, and A. E. Carlsson, Phys. Rev. B **37**, 4137 (1988).

[9]B. E. Larson, K. C. Hass, and R. L. Aggarwal, Phys. Rev. B **33**, 1789 (1986).

[10]Y. Shapira and N. F. Olivera, Jr., Phys. Rev. B **35**, 6888 (1987).

[11]For a review of spin glasses see K. Binder and A. P. Young, Rev. Mod. Phys. **58**, 801 (1986).

[12]DM interactions in metallic spin glasses have proved to be important in understanding anisotropy and hysteresis: J. J. Prejean, M. Joliclerc, and P. Monod, J. Phys. (Paris) **41**, 427 (1980); K. Okuda and M. Date, J. Phys. Soc. Jpn. **27**, 839 (1969); P. Monod and Y. Berthier, J. Magn. Magn. Mater. **15-18**, 149 (1980); P. M. Levy, C. Morgan-Pond, and R. Raghavan, Phys. Rev. Lett. **50**, 1160 (1983); Phys. Rev. B **30**, 2358 (1984); C. L. Henley, H. Sompolinsky, and B. I. Halperin, *ibid.* **25**, 5849 (1982).

[13]Simulations suggest anisotropic interactions may be needed for vector spins to undergo a spin-glass transition: R. E. Walstedt and L. R. Walker, Phys. Rev. Lett. **47**, 1624 (1981); K. Binder and W. Kinzel, J. Phys. Soc. Jpn. **52**, S-209 (1983); R. F. Angulo and J. F. Fernandez, J. Phys. C **20**, 1495 (1987); and T. M. Giebultowicz, B. Lebech, B. Buras, W. Minor, H. Kepa, and R. R. Galazka, J. Appl. Phys. **55**, 2305 (1984).

[14]An optical magnetic-field sensor has been described by M. A. Butler, Bull. Am. Phys. Soc. **32**, 912 (1987).

[15]The isotropic exchange calculations and related calculations of the (*sp* band)-Mn exchange are briefly described in, B. E. Larson, K. C. Hass, H. Ehrenreich, and A. E. Carlsson, Solid State Commun. **56**, 347 (1985); J. Magn. Magn. Mater. **54-57**, 1283 (1986).

[16]K. C. Hass, H. Ehrenreich, and B. Velicky, Phys. Rev. B **27**, 1088 (1983).

[17]A. Fert and P. M. Levy, Phys. Rev. Lett. **49**, 1508 (1980); J. Appl. Phys. **52**, 1718 (1981).

[18]See, e.g., L. D. Landau and E. M. Lifshitz, *Quantum Mechanics*, 3rd ed. (Pergamon, Oxford, 1977), p. 266.

[19]J. J. Pearson, Phys. Rev. **126**, 901 (1962).

[20]A. Baldereschi, Phys. Rev. B **7**, 5212 (1973).

[21]D. J. Chadi and Marvin L. Cohen, Phys. Rev. B **7**, 692 (1973); **8**, 5747 (1973).

[22]D. J. Chadi, Phys. Rev. B **16**, 790 (1977). The values have

been rescaled by $\sim 10\%$ to bring the CdTe value in line with that determined in Ref. 16.

[23]C. J. Gorter and J. H. Van Vleck, Phys. Rev. **72**, 1128 (1947).

[24]A. Abragam and B. Bleaney, *Electron Paramagnetic Resonance of Transition Ions* (Dover, New York, 1986), corrected edition.

[25]J. H. Van Vleck, Phys. Rev. **74**, 1168 (1948).

[26]R. E. Kremer and J. K. Furdyna, Phys. Rev. B **31**, 1 (1985).

[27]N. Samarth and J. K. Furdyna, Solid State Commun. **65**, 801 (1988); N. Samarth, Ph.D. thesis, Purdue University, 1986. We thank the authors for permission to use prepublication data.

[28]P. W. Anderson and P. R. Weiss, Rev. Mod. Phys. **25**, 269 (1953); R. Kubo and K. Tomita, J. Phys. Soc. Jpn. **9**, 888 (1954).

[29]P. A. Fedders, Phys. Rev. B **3**, 2352 (1971).

[30]C. Shannon, Bell Syst. Tech. J. **27**, 379 (1948); **27**, 623 (1948).

[31]E. T. Jaynes, Phys. Rev. **106**, 620 (1957); **108**, 171 (1957).

[32]L. R. Mead and N. Papanicoulau, J. Math. Phys. **25**, 2404 (1984).

[33]P. A. Fedders and A. E. Carlsson, Phys. Rev. B **32**, 229 (1985).

[34]A survey of the *phenomenological* equations used previously to fit the temperature dependence is given in Ref. 1.

[35]S. B. Oseroff, Phys. Rev. **25**, 6584 (1982).

[36]H. A. Sayad and S. M. Bhagat, Phys. Rev. B **31**, 591 (1985).

[37]K. C. Hass and H. Ehrenreich, J. Vac. Sci. Technol. A **1**, 1678 (1983).

[38]H. Ehrenreich, K. C. Hass, N. F. Johnson, B. E. Larson, and R. J. Lempert, in *Proceedings of the 18th International Conference on the Physics of Semiconductors,* edited by O. Engström (World Scientific, Stockholm, 1987), Vol. 2, p. 1751.

[39]H. Ehrenreich, K. C. Hass, B. E. Larson, and N. F. Johnson, in *Proceedings of the MRS Symposium on Diluted Magnetic (Semimagnetic) Semiconductors, Boson, 1986,* edited by R. L. Aggarwal, J. K. Furdyna, and S. von Molnar (Materials Research Society, Boston, 1987), p. 187.

[40]B. Vélicky, J. Mašek, V. Chab, and B. A. Orlowski, Acta Phys. Pol. A **69**, 1059 (1986).

[41]Atomic spectra indicate that other occupations (d^3,d^7) involve large energy costs. [C.E. Moore, *Atomic Energy Levels* (U.S. GPO, Washington, D.C., 1971), Vol. II.]

[42]See, e.g., the review articles cited in the Introduction, and also S. B. Oseroff, R. Calvo, W. Giriat, and Z. Fisk, Solid State Commun. **35**, 539 (1980).

[43]J. C. Slater and G. F. Koster, Phys. Rev. **94**, 1498 (1954).

[44]W. A. Harrison, *Electronic Structure and the Properties of Solids* (Freeman, San Francisco, 1980).

[45]J. A. Gaj, R. Planel, and G. Fishman, Solid State Commun. **29**, 435 (1979).

[46]One must include all allowable permutations of spin-conserving versus spin-flipping transfers. For example, in *CDAB*, the *D* transfer as diagrammed is not possible before *A*. In this case the *CD* transfer becomes spin flipping and subsequent *AB* transfer spin conserving.

[47]J. C. Phillips, Comments Solid State Phys. **4**, 115 (1973).

[48]F. Keffer, Phys. Rev. **126**, 896 (1962).

[49]See, e.g., J. D. Jackson, *Classical Electrodynamics* (Wiley, New York, 1975).

[50]R. S. Title, Phys. Rev. **131**, 2503 (1963), and references therein.

[51]J. Lambe and C. Kikuchi, Phys. Rev. **119**, 1256 (1960).

[52]P. B. Dorain, Phys. Rev. **112**, 1058 (1958).

[53]T. Grochulski, K. Liebler, A. Sienkiewicz, and R. R. Galazka, Phys. Status Solidi B **91**, K73 (1979).

[54]S. B. Oseroff, R. Calvo, and W. Giriat, J. Appl. Phys. **50**, 7738 (1979); Ref. 35 and S. B. Oseroff, R. Calvo, Z. Fisk, and F. Acker, Phys. Lett. **80**, 311 (1980).

[55]D. P. Mullin, R. R. Galazka, and J. K. Furdyna, Phys. Rev. B **23**, 1384 (1981).

[56]A. Manoogian, B. W. Chan, R. Brun del Re, T. Donofrio, and J. C. Wolley, J. Appl. Phys. **53**, 8934 (1982).

[57]D. J. Webb, S. M. Bhagat, and J. K. Furdyna, J. Appl. Phys. **55**, 2310 (1984).

[58]P. C. Martin, in *Many-Body Physics,* edited by C. DeWitt and R. Balian (Gordon and Breach, New York, 1968).

[59]D. Forster, *Hydrodynamic Fluctuations, Broken Symmetry, and Correlation Functions* (Benjamin/Cummings, London, 1975).

[60]R. Zwanzig, Phys. Rev. **124**, 983 (1961); H. Mori, Prog. Theor. Phys. (Kyoto) **33**, 423 (1965); **34**, 399 (1965).

[61]W. Götze and P. Wölfle, J. Low Temp. Phys. **5**, 575 (1971).

[62]Note that the sum rule $\chi_0=\int(\omega\pi)^{-1}\chi''(\omega)d\omega$ implies $M_0=1$. For nonzero ω_0 the peak [in $\chi_{\mathcal{M}^+,\mathcal{M}^-}(\omega)$; $\mathcal{M}^{\pm}=\mathcal{M}_x\pm i\mathcal{M}_y$] is centered at ω_0 about which M_n and L_n must then be computed. Assuming the line remains symmetric about its center, as seen in experiment (Ref. 27), one can carry out the calculation of moments by canonical transformation to a frame rotating at ω_0. The principal results are $M_2^{\infty}(\omega_0)=M_2^{\infty}(0)$, while $M_4^{\infty}(\omega_0)=M_4^{\infty}(0)(1+C\omega_0/\omega_e)$, where C is a constant of order unity and ω_e is the exchange frequency defined in Eq. (3.28). Thus the linewidth is unchanged from its zero-field value when $\omega_0\ll\omega_e\sim J_1$.

[63]Y. Shapira, S. Foner, D. H. Ridgley, K. Dwight, and A. Wold, Phys. Rev. B **30**, 4021 (1984).

[64]See, e.g., N. W. Ashcroft and N. D. Mermin, *Solid State Physics* (Holt, Rinehart, and Winston, New York, 1976).

[65]For a recent review, see *The Maximum Entropy Formalism,* edited by R. D. Levine and M. Tribus (MIT, Cambridge, 1979).

[66]S. A. Trugman, Phys. Rev. Lett. **57**, 607 (1986).

[67]R. H. Brown and A. E. Carlsson, Phys. Rev. B **32**, 6125 (1985).

[68]A. E. Carlsson, Phys. Rev. Lett. **59**, 1108 (1987).

[69]The assumption of a Gaussian memory function parametrized by the second and fourth microscopic moments of the associated response function has been made previously. See Ref. 29 and D. Forster, P. C. Martin, and S. Yip, Phys. Rev. **170**, 155 (1968); **170**, 160 (1968).

[70]Mori (Ref. 60) shows that the memory function can be written as a response function for $\partial_t\mathcal{M}_x$ where the dynamics of $\mathcal{M}_x$ itself have been projected out. The maximum entropy method could also be applied directly to the response function $\chi''(\omega)$. Fedders and Carlsson (Ref. 33) obtained better results by working in terms of the memory functions, because of their smoother frequency dependence [Eq. (3.6)].

[71]This result agrees with the estimates made in Refs. 27 and 28.

[72]It is easy to verify that nothing essential to these estimates is changed if $H_{\rm dip}$ or $H_{\rm single}$ is the dominant anisotropic interaction. The DM coupling constant D_1 in e.g., Eq. (3.29), is replaced by the coupling constant $d_{\rm dip}$, or $D_{\rm single}$ (or $a_{\rm cub}$), respectively.

[73]C. Kittel and E. Abrahams, Phys. Rev. **90**, 238 (1953).

[74]D. U. Bartholomew, E. K. Suh, S. Rodriguez, A. K. Ramdas, and R. L. Aggarwal, Solid State Commun. **62**, 35 (1987).

[75]D. R. Yoder-Short, U. Debska, and J. K. Furdyna, J. Appl. Phys. **58**, 4056 (1985), and references therein.

[76]The approximate nature of the corrections $\delta\Delta H_{\infty}$, which

comprise the majority of the $Cd_{1-x}Mn_xS$ linewidth, naturally makes the agreement with experiment less good for this material.

[77]P. M. Levy and R. Raghavan, J. Magn. Magn. Mater. **54- 57**, 181 (1986).

[78]J. E. Gulley, D. Hone, D. J. Scalapino, and B. G. Silbernagel, Phys. Rev. B **1**, 1020 (1970).

[79]J. Spałek, A. Lewicki, Z. Tarnawski, J. K. Furdyna, R. R. Galazka, and Z. Obuszko, Phys. Rev. B **33**, 3407 (1986).

[80]A standard least-squares statistical method is used. See P. R. Bevington, *Data Reduction and Error Analysis for the Physical Sciences* (McGraw-Hill, New York, 1969).

[81]We have linearly interpolated Θ_p^{ex} for some intermediate concentrations.

[82]The errors here are statistical. The experimental errors in $\Delta H(T)$ measurements are all $\sim 5\%$ (Refs. 27, 35, and 36).

[83]$\Delta H(T)$ is calculated using the experimental Θ_p^{ex} and calculated ΔH_∞ and Θ_2, with ΔH_∞ calculated analogously to the entries in line 3 of Table II.

[84]Temperature-dependent EPR data of $300 \leq T \leq 1000$ K for the fcc antiferromagnets MnO and α-MnS are consistent with $\Theta_d \ll \Theta_p$ [E. Dormann and V. Jaccarino, Phys. Lett. **48A**, 81 (1974)].

[85]M. Taniguchi, L. Ley, R. L. Johnson, J. Ghijsen, and M. Cardona, Phys. Rev. B **33**, 1206 (1986).

[86]A. Franciosi, S. Chang, R. Reifenberger, U. Debska, and R. Riedel, Phys. Rev. B **32**, 6682 (1985).

[87]M. Taniguchi, M. Fujimori, M. Fujisawa, T. Mori, I. Souma, and Y. Oka, Solid State Commun. **62**, 431 (1987).

[88]A. Franciosi, in Ref. 39, p. 175.

[89]A. Franciosi, S. Chang, C. Caprile, R. Reifenberger, and U. Debska, J. Vac. Sci. Technol. A **3**, 926 (1985).

[90]P. Lautenschlager, S. Logothetidis, L. Viña, and M. Cardona, Phys. Rev. B **32**, 3811 (1985).

[91]R. L. Aggarwal, S. N. Jasperson, P. Becla, and R. R. Galazka, Phys. Rev. B **32**, 5132 (1985).

[92]D. Heiman, Y. Shapira, and S. Foner, Solid State Commun. **51**, 603 (1984), and references therein.

[93]A. Twardowski, T. Dietl, and M. Demianiuk, Solid State Commun. **48**, 845 (1983).

[94]Y. Shapira, D. Heiman, and S. Foner, Solid State Commun. **44**, 1243 (1982).

[95]R. L. Aggarwal, S. N. Jasperson, J. Stankiewicz, Y. Shapira, S. Foner, B. Khazai, and A. Wold, Phys. Rev. B **28**, 6907 (1983).

[96]M. Nawrocki, J. P. Lascaray, D. Coquillat, and M. Demianiuk, in Ref. 39, p. 65.

[97]A. Twardowski, P. Swiderski, M. von Ortenburg, and R. Pauthenet, Solid State Commun. **50**, 509 (1984).

[98]G. Barilero, C. Rigaux, M. Menant, Nguyen Hy Hau, and W. Giriat, Phys. Rev. B **32**, 5144 (1986).

[99]A. Twardowski, M. von Ortenburg, M. Demianiuk, and R. Pauthenet, Solid State Commun. **51**, 849 (1984).

[100]J. P. Lascaray, M. Nawrocki, J. M. Broto, M. Rakoto, and M. Demianiuk, Solid State Commun. **61**, 401 (1987).

[101]L. M. Corliss, J. M. Hastings, S. M. Shapiro, Y. Shapira, and P. Becla, Phys. Rev. B **33**, 608 (1986).

[102]G. Barilero, C. Rigaux, Nguyen Hy Hau, J. C. Picoche, and W. Giriat, Solid State Commun. **62**, 345 (1987).

[103]T. M. Giebultowicz, J. J. Rhyne, and J. K. Furdyna, J. Appl. Phys. **61**, 3537 (1987).